

Composition and volatility of SOA formed from oxidation of real tree emissions compared to single VOC-systems

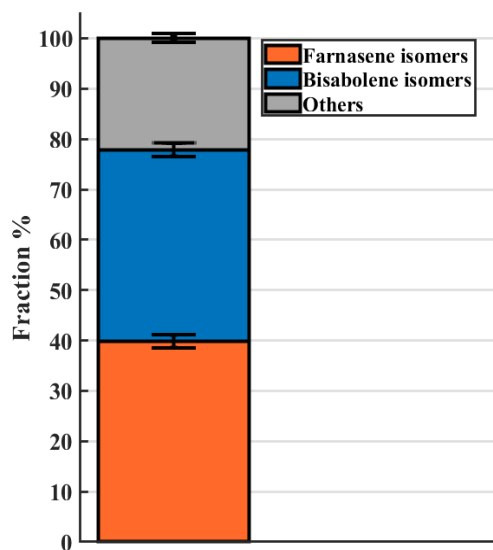
Arttu Ylisirniö et. al.,

5

S1. Sesquiterpene mixture and Scots pine emission description

Table S1. Identified compounds and their relative contributions to the sesquiterpene mixture, based on GC-MS analysis.

Compound	Fraction %
cis - β -farnesene	7.89 ± 0.44
(E) - β -farnesene	9.56 ± 0.11
(Z.Z) - α -farnesene	8.47 ± 0.24
(E.Z) - α -farnesene	7.25 ± 0.08
cis - α -farnesene	6.69 ± 0.29
trans - α - bisabolene	5.46 ± 0.38
β - bisabolene	9.73 ± 0.19
trans - γ -bisabolene	4.51 ± 0.11
cis - α -bisabolene	18.31 ± 0.64
unidentified SQT	4.49 ± 0.10
unidentified SQT	3.98 ± 0.29
unidentified SQT	5.95 ± 0.13
unidentified SQT	7.73 ± 0.11



10

Figure S1: Graphical representation of data from Table S1, where different isomers of farnesene and bisabolene are summed up together. Unidentified compounds are summed into others class.

Table S2. Identified compounds and their relative contributions to the Scots pine emissions, based on GC-MS analysis.

Monoterpenes	Fraction from total emission % (Scots pine exp. 1)	Fraction from total emission % (Scots pine exp. 4)
β -Phellandrene	13.11 \pm 0.56	30.87 \pm 12
3-Carene	9.22 \pm 0.8	15.42 \pm 1.44
d-Limonene	8.40 \pm 0.87	12.68 \pm 3.01
β -Pinene	7.13 \pm 0.42	7.98 \pm 3.36
α -Pinene	4.29 \pm 0.17	6.99 \pm 1.64
Myrcene	1.17 \pm 0.24	2.62 \pm 0.34
Terpinolene	1.15 \pm 1.07	1.58 \pm 1.32
Camphene	0.61 \pm 0.02	1.93 \pm 0.3
o-Cymene	0.47 \pm 0.07	0.7 \pm 0.13
α -Phellandrene	0.43 \pm 0.6	0.6 \pm 0.27
γ -Terpinene	0.21 \pm 0.14	0.77 \pm 0.36
Cymenene	0.17 \pm 0.06	0.36 \pm 0.01
Trans- β -Ocimene	0.09 \pm 0.05	0.1 \pm 0.02
α -Fenchene	0.05 \pm 0.01	0.05 \pm 0.01
Sabinene	0.03 \pm 0.01	0.06 \pm 0.01
Sesquiterpenes	Fraction from total emission % (Scots pine exp. 1)	Fraction from total emission % (Scots pine exp. 4)

Trans- β -Farnesene	41.17 \pm 0.58	14.3 \pm 4.68
α -Farnesene	9.81 \pm 0.95	1.83 \pm 0.73
α -Bisabolene	2.13 \pm 0.14	0.61 \pm 0.14
aromadendrene	0.14 \pm 0.07	0.09 \pm 0.06
β -Caryophyllene	0.06 \pm 0.04	0.12 \pm 0.07
α -Humulene	0.06 \pm 0.03	0.15 \pm 0.04
α -Copaene	0.06 \pm 0.01	0.09 \pm 0.01
β -Elemene	0.03 \pm 0.01	0.02 \pm 0.01
Longifolene	0.01 \pm 0.01	0

15 S2. PTR-ToF-MS calibration

The PTR-ToF-MS was calibrated using a calibration gas standard with 8 aromatic compounds of mixing ratios ~100 ppbv in nitrogen (BOC, United Kingdom). The same gas standard was used to correct for non-ideal transmission in the instrument. Monoterpene and sesquiterpene concentrations were estimated from the Scots pine emission data using the ion signals of the protonated compounds at m/z 137 for monoterpenes and m/z 205 for sesquiterpenes, and accounting for the fragmentation of these ions by applying factors of 0.478 for monoterpenes and 0.5 for sesquiterpenes (compare (Kari et. al., 2018)).

S3. FIGAERO-CIMS calibration

The FIGAERO-CIMS mass axis was calibrated using known reagent ions and background signals, such as I , H_2OI , HNO_3I , I_2 , I_3 . Sensitivity calibration was not performed as each observed molecule should have been identified and calibrated individually, which was not possible with the experimental setup our study is based on. We therefore mostly show normalized data.

The conversion from peak desorption temperatures T_{max} to saturation vapor pressure P_{sat} and from there to saturation vapor concentration C^* was performed using a modified calibration method based on Bannan et al. (2018), using a series of polyethylene glycols (PEG) as reference compounds. Details of that modification will be published shortly in a separate publication. Calibration was done by fitting eq. S1 to measured values of T_{max} and literature-based values of P_{sat} for the PEGs:

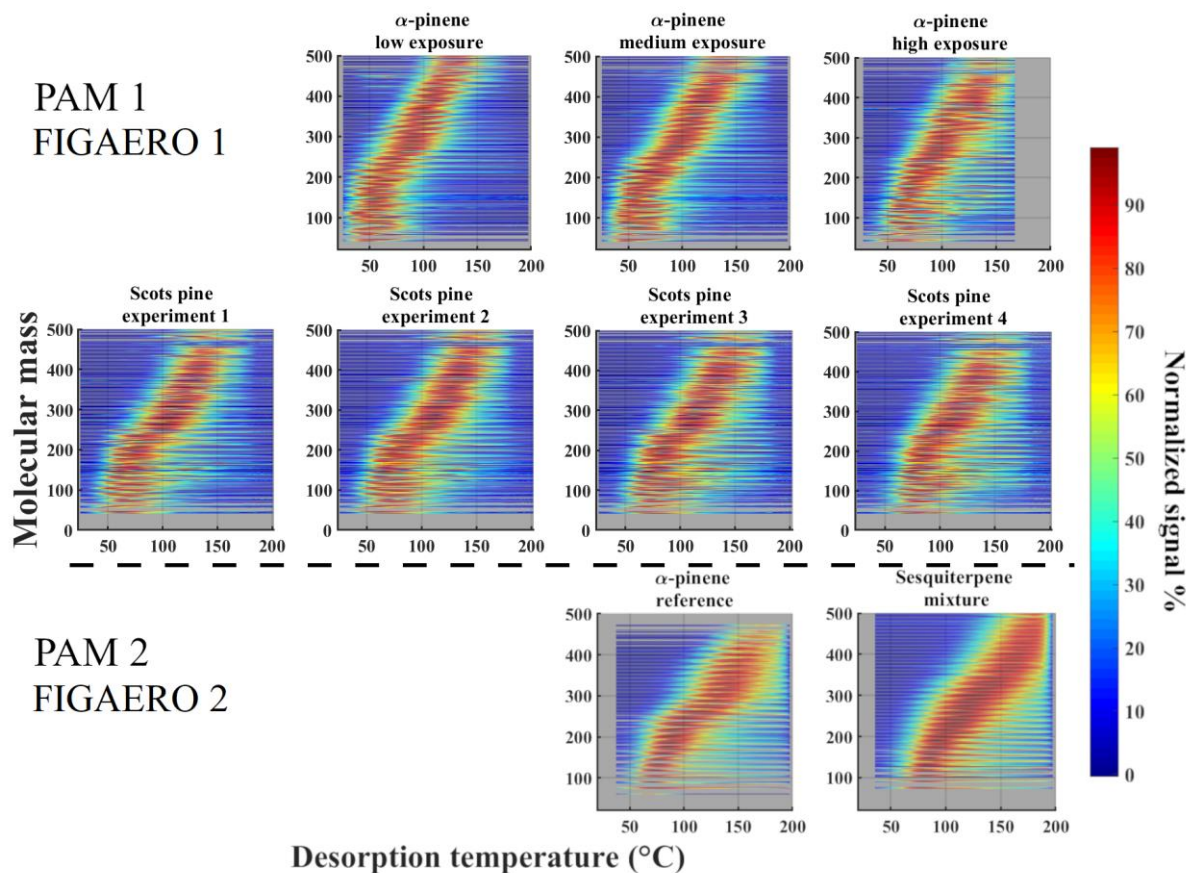
$$P_{sat} = \exp(bT_{max} + a), \quad (S1)$$

where a and b are fitting coefficients. These coefficients were the following for FIGAERO inlets 1 and 2:

- 35 FIGAERO 1: $a = -1.431$, $b = -0.207$
 FIGAERO 2: $a = -3.929$, $b = -0.132$.

P_{sat} was then converted to C^* with the assumptions of the ideal gas law.

40 S4. Extended discussion of SOA volatility



45 **Figure S2: Individual ions' thermograms from each experiment, each depicted as a separate two-dimensional, colored plot. The x-axes show desorption temperature; y-axes nominal (integer) ion mass. For clarity, signals have been summed up for each nominal mass, and colors show the intensity of said nominal mass normalized to the respective thermogram's maximum signal. Top row: α -pinene experiments (cf. Fig. 5a). Middle row: Scots pine experiments (cf. Fig. 5b). Bottom row: experiments using PAM 2 (sesquiterpene mixture and reference α -pinene experiment; cf. Fig. 5c).**

50 Figure S2 reveals that the T_{max} value of detected ions are in general dependent on their molecular weight, as is expected. However, this dependence tends to disappear for ions corresponding to compounds with molecular weights less than around 150 Da, and their T_{max} tend to fall inside the same range. On the one hand, that is likely a form of observational bias, as at this lower molecular weight range, only relatively lower-volatility compounds would partition into the particle phase. On the other hand, as mentioned above, we can expect at least some compounds with lower molecular weights to be products of thermal decomposition of larger compounds. More apparent signatures of thermal decomposition are visible as well: thermograms peaking at clearly higher temperatures than expected by the respective molecular weight, and thermograms

substantially extending towards higher temperatures (tailing). Both of those signatures have also been extensively observed
55 also in previous studies (Wang et al., 2016, D'Ambro et al., 2017; Lopez-Hilfiker et al., 2014; Lopez-Hilfiker et al., 2015;
Lopez-Hilfiker et al., 2016; Schobesberger et al., 2018).

The top row of Fig. S2 shows that not only do the sum thermograms for the α -pinene experiments shift to higher desorption
60 temperatures with increasing oxidation exposure, but the shift is essentially seen throughout the spectrum of individual
thermograms (cf. Fig. 5). In addition, an increasing role of thermal decomposition is apparent, especially through increasing
tailing of the thermograms. In the same manner, T_{max} values are increased throughout the spectrum when comparing the
reference α -pinene to the sesquiterpene mixture experiment (bottom row Fig. S2), with notable contributions of
75 decomposition processes in both cases. In line with these observations, and those in Figs. 4-5, the plots obtained from the
Scots pine experiments (middle row Fig. S2) broadly appear as expected: as in-between cases between the α -pinene and the
sesquiterpene results. As in Fig. 5, Scots pine experiment 4 features the highest T_{max} values, and also somewhat larger
apparent contributions by thermal decomposition products. But overall, the similarities to the other Scots pine experiments
(especially experiment 3) predominate (cf. Fig. 4), in spite of the much higher contribution of monoterpenes than in
80 experiments 1-3.

References:

- 70 Ambro, E. L. D., Lee, B. H., Liu, J., Shilling, J. E., Gaston, C. J., Lopez-hilfiker, F. D., Schobesberger, S., Zaveri, R. A.,
Mohr, C., Lutz, A., Zhang, Z., Gold, A., Surratt, J. D., Rivera-rios, J. C., Keutsch, F. N. and Thornton, J. A.: Molecular
composition and volatility of isoprene photochemical oxidation secondary organic aerosol under low- and high-NO_x
conditions, , 159–174, doi:10.5194/acp-17-159-2017, 2017.
- Bannan, T. J., Le Breton, M., Priestley, M., Worrall, S. D., Bacak, A., Marsden, N. A., Merha, A., Hammes, J., Hallquist,
75 M., Alfarra, M. R., Krieger, U. K., Reid, J. P., Jayne, J., Robinson, W., Mcfiggans, G., Coe, H., Percival, C. J. and Topping,
D.: A method for extracting calibrated volatility information from the FIGAERO-HR-ToF-CIMS and its application to
chamber and field studies, , (August), 1–12, doi:10.5194/amt-2018-255, 2018.
- Kari, E., Miettinen, P., Yli-Pirilä, P., Virtanen, A. and Faiola, C. L.: PTR-ToF-MS product ion distributions and humidity-
dependence of biogenic volatile organic compounds, Int. J. Mass Spectrom., 430, 87–97, doi:10.1016/j.ijms.2018.05.003,
80 2018.
- Lopez-Hilfiker, F. D., Mohr, C., Ehn, M., Rubach, F., Kleist, E., Wildt, J., Mentel, T. F., Lutz, A., Hallquist, M., Worsnop,
D. and Thornton, J. A.: A novel method for online analysis of gas and particle composition: Description and evaluation of a
filter inlet for gases and AEROSols (FIGAERO), Atmos. Meas. Tech., 7(4), 983–1001, doi:10.5194/amt-7-983-2014, 2014.
- Lopez-Hilfiker, F. D., Mohr, C., Ehn, M., Rubach, F., Kleist, E., Wildt, J., Mentel, T. F. and Carrasquillo, A. J.: Phase
85 partitioning and volatility of secondary organic aerosol components formed from α -pinene ozonolysis and OH oxidation :
the importance of accretion products and other low volatility, Atmos. Chem. Phys., 7765–7776, doi:10.5194/acp-15-7765-
2015, 2015.
- Lopez-Hilfiker, F. D., Iyer, S., Mohr, C., Lee, B. H., D'ambro, E. L., Kurtén, T. and Thornton, J. A.: Constraining the
sensitivity of iodide adduct chemical ionization mass spectrometry to multifunctional organic molecules using the collision
90 limit and thermodynamic stability of iodide ion adducts, Atmos. Meas. Tech., 9(4), 1505–1512, doi:10.5194/amt-9-1505-
2016, 2016.
- Schobesberger, S., D'Ambro, E. L., Lopez-Hilfiker, F. D., Mohr, C. and Thornton, J. A.: A model framework to retrieve
thermodynamic and kinetic properties of organic aerosol from composition-resolved thermal desorption measurements,
Atmos. Chem. Phys., 18(20), 14757–14785, doi:10.5194/acp-18-14757-2018, 2018.

- 95 Wang, M., Yao, L., Zheng, J., Wang, X., Chen, J., Yang, X., Worsnop, D. R., Donahue, N. M. and Wang, L.: Reactions of Atmospheric Particulate Stabilized Criegee Intermediates Lead to High-Molecular-Weight Aerosol Components, , doi:10.1021/acs.est.6b02114, 2016.